Available online at www.sciencedirect.com

ScienceDirect

Procedia Structural Integrity 39 (2022) 301–312

Structural Integrity Procedia

www.elsevier.com/locate/procedia

7th International Conference on Crack Paths

Assessment of multiaxial fatigue of crankshafts subjected to both designed and theoretically critical loadings

TL Castro[a,*], LC Araujo[b], TA Peixoto[a], BF Carvalho[a], MV Pereira[a], JA Araújo[b]

[a]*Department of Chemical and Materials Engineering, Pontifical Catholic University of Rio de Janeiro, Rua Marquês de São Vicente, 225, Rio de Janeiro, 22451-900, RJ, Brazil*

[b]*Department of Mechanical Engineering, University of Brasilia, Faculdade de Tecnologia, Campus Universitário Darcy Ribeiro, Asa Norte, Brasília, 70910-900, DF, Brazil*

Abstract

Fatigue failures of motor crankshafts operating in thermoelectric power plants are recently being reported. Since crankshafts are subjected to non-trivial stress states throughout their operation, multiaxial fatigue theory is required. A previously carried-out finite element analysis (FEM) that determined the stress states of critical points within the crankshaft's was used as input. Biaxial stress states were extracted from the FEM analysis and submitted to multiaxial fatigue testing. The fatigue behaviour of the given loading conditions was assessed by using seven multiaxial high-cycle fatigue criteria, namely Findley (F), Matake (M), McDiarmid (McD), Susmel & Lazzarin (S&L), Carpinteri & Spagnoli (C&S), Liu & Mahadevan (L&M) and Papadopoulos (P). An additional set of critical loading conditions was also considered and submitted to both fatigue testing and theoretical predictions. By using experimentally observed fatigue resistance limits, the predictions deliver a slight tendency to fatigue failure in their prediction, in contrast to experimental observations. The results were used to compare the prediction capability of the selected criteria, where all presented reasonably fair agreement. Within the present study's context, Papadopoulos' model was the one that presented the least spread in fatigue predictions while also presenting the closest to ideal average behaviour, with the convenient feature of being slightly conservative.

Keywords: Critical plane criteria; biaxial fatigue loadings; Non-trivial cyclic stress-states

* Corresponding author. Tel.: +55 21 9 8858 6220.
E-mail address: tiagocastrobl@gmail.com

10.1016/j.prostr.2022.03.100

1. Introduction

Fatigue is a well-known technical problem where damage is accumulated due to repeated application of stresses or strains which may induce crack nucleation, followed by crack propagation leading material to failure under loading conditions well below the static strength of the material in question (Suresh, 1998).

This issue became a subject of interest in a context when Europe was experiencing the industrial revolution. The increase in production was accompanied by an enhancement in the railroad network, where trains were operating for longer periods and travelling longer distances to meet the also growing demand in increasingly further markets.

In the mid-1800s, several fatigue failures were being reported, as axles began to present failures despite being subjected to loads far below the static strength of the material (Schijve, 2009). Within this context, the German engineer August Wöhler proposed the S-N curve, establishing a relation between the cyclic stress amplitude and the fatigue-life that such component is expected to endure. This breakthrough provided means to a better selection of materials, thus yielding a safer project design.

Many studies were dedicated to better understand the mechanisms that led to fatigue failures, and much has been learned. However, up to this date, the evaluation of fatigue behaviour of metallic materials is still very commonly addressed by using conventional uniaxial fatigue theory, which may not be the best suited approach to components that are known to experience non-trivial cyclic stress states throughout their operation.

Such conditions demand a more robust theoretical approach in order to adequately predict the fatigue behaviour of the component in question. Several multiaxial fatigue criteria have been proposed and are widely available in the literature (Marquis & Socie, 2000).

Regarding the context of this study, fatigue failures of motor crankshafts operating in thermoelectric power plants are recently being reported. Since thermoelectric power corresponds to a significant share of the Brazilian energetic matrix, the comprehension of such failures becomes of great importance.

Forged in 42CrMo4 steel, the material properties (endurance limits) were determined by the authors in recent studies (Castro, 2019; Machado et al., 2020). In addition, a finite element (FEM) analysis, which was previously carried out to determine the stresses acting on the crankshaft was also considered as input data for the present work.

Six critical plane-based multiaxial fatigue criteria, namely Findley (Findley, 1959), Matake (Matake, 1977), McDiarmid (McDiarmid, 1987), Susmel & Lazzarin (Susmel & Lazzarin, 2002), Carpinteri & Spagnoli (Carpinteri & Spagnoli, 2001) and Liu & Mahadevan (Liu & Mahadevan, 2005), as well as a mesoscopic scale-based criterion, namely Papadopoulos (Papadopoulos et al., 1997), were considered to evaluate whether such loadings are adequate to the materials which are used to forge the crankshafts.

Theoretical predictions were carried out by comparing the left-hand side (LHS) with the right-hand side (RHS) of the criteria's expressions, allowing one to assess whether or not such loading conditions are expected to drive material to fatigue failure. The mentioned relative difference defines the error index I, and the criteria's prediction are then compared to the experimental observations.

An additional set of critical loading conditions (Papadopoulos et al., 1997) was considered. Such loading conditions are expected to drive the material to the limiting state of fracture or non-fracture in the order of one million cycles. In theory, they should yield error indices that approximate zero, as the LHS (associated to the driving force to failure) should approach the RHS (which is associated to the material's fatigue resistance limit). However, by considering the experimentally obtained fatigue resistance limits (Castro, 2019; Machado et al., 2020), variations in the error indices may be expected, allowing one to adequately conclude over the conservativeness or non-conservativeness of the involved criteria.

2. Materials and methods

The present study considered specimens which were extracted from a crankshaft which presented early failure while in operation. Broadly speaking, the connecting rods of the crankshaft are attached to the pistons on one end and to the crankshaft's crankpin journals on the other. The up and down motion of the pistons inside the cylinder bores puts the crankpin journals into motion, as firing sequence imposes an adequate sequence of torques to the crankshaft making it revolve. Since the crankpin journals are offset to the main journal centreline (by what is known as the crank radius), the crankpins describe circles of their own.

The studied crankshaft has 10 crankpin journals, each one presenting 2 connecting rods assembled to it. The assembling points impose cyclic stresses to the crankshaft, yielding 20 different critical points along the crankshaft's length. The critical points in the crankpin journal are close to the spot where the connecting rods are connected, where a change in geometry can be observed, leading to geometric stress concentrators.

Crankpin journals are numbered from 1 to 10, while the critical points per crankpin are identified as A and B. Accordingly, the critical points throughout the crankshaft can be identified as A01, B01, A02, B02 and so on. Fig. 1 (a) and (b) illustrate the crankshaft, where the relevant parts are identified, while Fig. 2 depicts fatigue crack in the crankpin journal (which nucleated on the critical point) and how it propagated.

2.1. Input data

The crankshaft was forged in DIN 42CrMo4 steel, with the chemical composition and mechanical properties presented in Table 1 (Peixoto, 2018) and Table 2 (Castro, 2019; Machado et al., 2020). Scanning electron microscopy (SEM) revealed 95 particles/mm^2 (non-metallic inclusions) and the threshold stress intensity factor for crack propagation was experimentally determined as $\Delta K_{th} = 10.50\ \mathrm{MPa}\sqrt{\mathrm{m}}$ (Peixoto, 2018).

a b

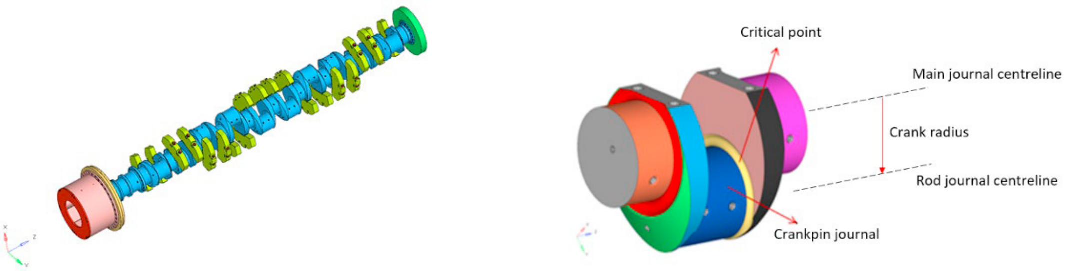

Fig. 1. (a) Illustration of the crankshaft; (b) identification of the relevant parts

a b

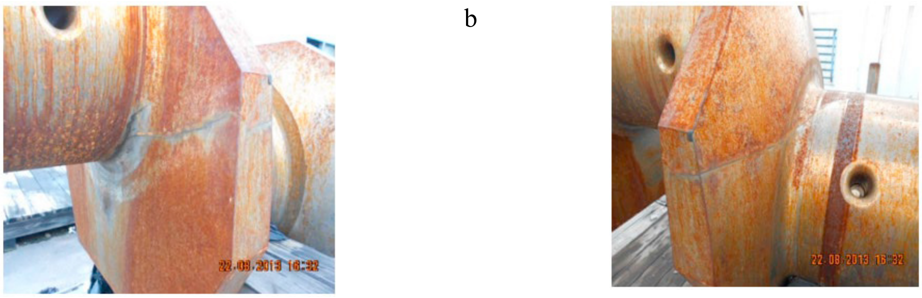

Fig. 2. (a) Fatigue crack nucleation spot; (b) fatigue crack path

Using strain data that was obtained from the crankshaft while in operation, a finite element analysis method prior to the present study was carried out, and the obtained stresses acting on the 20 critical points along the crankshaft were considered as input data (Schwaben, 2015).

The full cycle of the considered crankshaft involves 2 complete revolutions of the axis (720°). For considered increments in angular position of 1 degree, for each angular position the critical points are subjected to a different stress state. Thus, each critical point yields 720 stress tensors within a full cycle of the crankshaft. Fig. 3 depicts the stresses acting on the critical point B06.

Table 1. Chemical composition of the DIN 42CrMo4 steel (Peixoto, 2018)

DIN 42CrMo4								
Fe (%)	**C (%)**	**Mn (%)**	**Si (%)**	**Cu (%)**	**Cr (%)**	**V (%)**	**Mo (%)**	**Ni (%)**
96,9	0,38	0,85	0,27	0,18	0,97	0,01	0,2	--

Table 2. Mechanical properties of the DIN 42CrMo4 steel (Castro, 2019; Peixoto, 2018)

Mechanical property	
Yield stress, σ_y	$715\ MPa$
Ultimate tensile stress, σ_u	906 MPa
Young's modulus, E	210 GPa
Fatigue resistance limit (bending), f_{-1}	357 MPa
Fatigue resistance limit (torsion), t_{-1}	275 MPa
Threshold stress intensity factor, ΔK_{th}	$10.50\ MPa\sqrt{m}$

2.2. Experimental scenario

Experiments were carried out at University of Brasilia (UnB), using a MTS-809 axial/torsional test system, depicted in Fig. 4. The load cell manages to apply 100 kN and 1100 Nm. Experiments were conducted with frequencies between 10 Hz to 15 Hz.

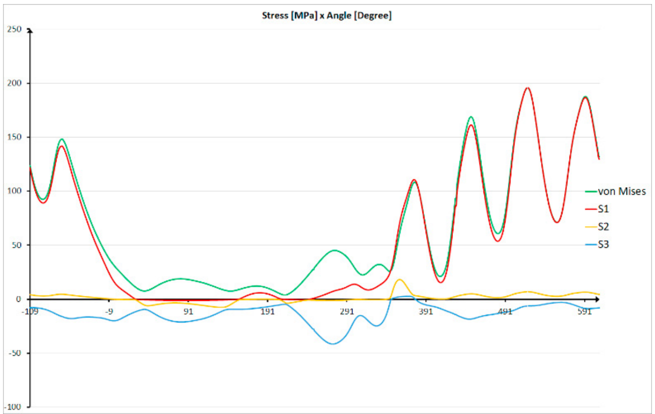

Fig. 3 – Stresses acting on critical point B06 throughout the 720° cycle of the crankshaft

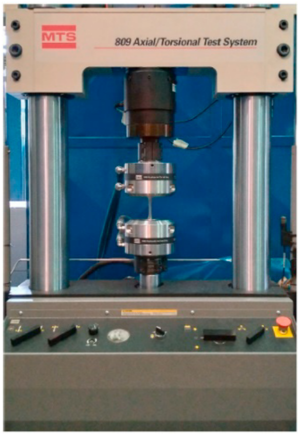

Fig. 4 – Axial/torsional fatigue testing system at University of Brasilia (UnB)

Since the testing system can only simultaneously apply an axial and a torsional load, an adequate methodology is required to translate the FEM-extracted stresses into a loading condition that can be experimented.

For each critical point, the maximum and the minimum principal stress were collected, allowing one to determine a stress amplitude $\sigma_a = (\max \sigma_1 - \min \sigma_1)/2$ and a mean normal stress $\sigma_m = (\max \sigma_1 + \min \sigma_1)/2$. The shear stress amplitude, in turn, was obtained by inspecting the maximum value of $\tau_a=(\sigma_1-\sigma_3)/2$. Since a superimposed mean shear stress should not affect the fatigue resistance limit in very high cycle fatigue, the present study considered the shear stress amplitude as equivalent to the maximum observed value of $(\sigma_1 - \sigma_3)/2$. The described procedure applied to B10 is illustrated in Fig. 5.

							B10					
Angle	node	VonMises	σxx	σyy	σzz	τxy	τyz	τxz	S1	S2	S3	τ_max
43	17758033	77,995	-19,82	-22,1	-78,98	6,042	23,79	17,376	-3,651	-26,68	-90,566	43,4575
44	17758033	78,146	-19,82	-22,18	-79,12	6,061	23,903	17,327	-3,657	-26,72	-90,738	43,5405
45	17758033	78,263	-19,81	-22,25	-79,22	6,077	24,005	17,27	-3,661	-26,75	-90,87	43,6045
46	17758033	78,342	-19,78	-22,31	-79,29	6,089	24,095	17,204	-3,664	-26,76	-90,957	43,6465
47	17758033	78,382	-19,75	-22,36	-79,31	6,099	24,173	17,13	-3,665	-26,76	-91	43,6675
48	17758033	78,385	-19,71	-22,4	-79,3	6,105	24,239	17,048	-3,664	-26,75	-90,998	43,667
49	17758033	78,351	-19,66	-22,43	-79,25	6,108	24,293	16,958	-3,662	-26,72	-90,953	43,6455
50	17758033	78,283	-19,6	-22,45	-79,16	6,109	24,336	16,862	-3,657	-26,68	-90,87	43,6065
Angle	node	VonMises	σxx	σyy	σzz	τxy	τyz	τxz	S1	S2	S3	τ_max
424	17758033	158,417	38,852	47,387	159,89	-13,28	-51,52	-31,17	184,065	54,674	7,39	88,3375
425	17758033	163,12	39,748	48,95	164,49	-13,68	-53,36	-31,66	189,474	56,113	7,601	90,9365
426	17758033	166,892	40,39	50,247	168,13	-13,99	-54,93	-31,93	193,793	57,206	7,767	93,013
427	17758033	169,603	40,749	51,237	170,68	-14,22	-56,17	-31,96	196,871	57,909	7,882	94,4945
430	17758033	170,55	39,985	52,084	170,97	-14,3	-57,63	-30,49	197,725	57,43	7,888	94,9185
431	17758033	168,37	39,111	51,617	168,53	-14,12	-57,31	-29,5	195,101	56,384	7,773	93,664
432	17758033	164,99	37,949	50,783	164,87	-13,84	-56,58	-28,29	191,08	54,919	7,601	91,7395

Fig. 5. Procedure to determine the biaxial stresses relative to critical point B10

The stresses are summarised into Table 3, which correspond to the most severe loading conditions extracted from the FEM. Lower loading conditions were discarded, as they were very unlikely to drive the specimens into fatigue failure. The apostrophe indicates the presence of a mean normal stress.

The most severe loading conditions, one in-phase (B06’) and another one out-of-phase (B03’), were selected to be the first ones to be experimented. Each loading condition should be tested at least twice, and the run-out limit was defined as 10 million cycles. Phase differences larger than 359° are a consequence of the fact that the full cycle of the crankshaft requires 2 whole revolutions. Authors were aware of the fact that this would have to be addressed should the necessity arise.

Table 3. FEM-extracted loading conditions

Loading condition	σ_a [MPa]	σ_m [MPa]	$\tau_a=(\sigma_1-\sigma_3)/2$ [MPa]	β [°]
B03'	54.12	41.31	111.60	235
B05'	50.08	48.86	85.09	447
A06'	71.12	62.77	82.22	293
B06'	98.23	97.41	100.91	0
A07'	80.51	79.18	88.11	1
B10'	100.70	97.03	94.92	0

Presented in Table 4, two additional loading conditions B06 and B03, which are correlated to B06' and B03', are presented. The difference is that B06 and B03 maintain the highest stress levels of B06' and B03', but they are fully reversed loading conditions, i.e., there is no mean normal stress involved. This approach neglects the effect of the normal mean stress, but in turn yields a much larger stress amplitude.

Being slightly more severe than the ones including mean normal stress, B06 and B03 were to be put to test in case both specimens of B06' and both specimens of B03' yield run-outs, as an attempt to verify how far B06' and B03' are from a critical state of failure due to fatigue.

Table 4. FEM-extracted loading conditions without mean normal stress

	σ_a [MPa]	$\tau_a=(\sigma_1-\sigma_3)/2$ [MPa]	σ_a [MPa]
B03	95.43	111.60	235
B06	195.63	85.09	0

2.3. Critical loading conditions

Relative to the 42CrMo4 steel, a critical set of loading conditions was firstly reported by Zenner (Zenner et al., 1985) and further replicated by Papadopoulos (Papadopoulos et al., 1997). These loading conditions are expected to drive the 42CrMo4 steel into the limiting state of fatigue failure in the order of 1 million cycles, and they may well serve as a benchmark comparison for the FEM-extracted loading conditions.

Six critical plane-based criteria were selected, namely Findley, Matake, McDiarmid, Susmel & Lazzarin, Carpinteri & Spagnoli, Liu & Mahadevan, as well as a mesoscopic scale-based criterion, namely Papadopoulos. Even though the latter is independent of critical plane determination, which makes it unique relative to the others, all the mentioned criteria work in a similar manner, which is by comparing the relative difference between the left-hand side (LHS) of the equation, associated to the driving force to fatigue failure, with the right-hand side (RHS) of the equation, associated to the materials fatigue resistance limit.

The error index I, presented in eq. (1), can be defined to assess the relative difference between LHS and RHS. It is important to point out that positive values of I indicate that the driving force to failure exceeds the material's fatigue resistance limit, suggesting that fatigue failures is likely to take place. On the other hand, negative values of I indicate that the materials resistance to fatigue is greater than the driving force to failure, and thus no fatigue failure should be expected.

$$I = \frac{LHS - RHS}{RHS} \tag{1}$$

The critical loading conditions in question are available in Table 5. Since they are expected to drive the material into a critical state in the eminence of fatigue failure, it is expected to achieve a situation where LHS equals the RHS, thus yielding $I=0$. While this statement may be true, it is only applicable to the theoretical fatigue resistance limits that are available in the literature, which are $f_{-1} = 398$ MPa and $t_{-1} = 260$ MPa, respectively for bending and torsion conditions.

Table 5. Additional set of critical loading conditions for 42CrMo4 (Papadopoulos et al., 1997; Zenner et al., 1985)

	σ_a [MPa]	σ_a [MPa]	τ_a [MPa]	τ_m [MPa]	σ_a [MPa]
A	328	0	157	0	0
B	286	0	137	0	90
C	233	0	224	0	0
D	213	0	205	0	90
E	266	0	128	128	0
F	283	0	136	136	90
G	333	0	160	160	180
H	280	280	134	0	0
I	271	271	130	0	90

Considering the experimentally measured fatigue resistance limits in fully reversed pure bending, $f_{-1} = 357$ MPa, and fully reversed pure torsion, $t_{-1} = 275$ MPa, a slight reduction in the overall fatigue resistance of the material should be expected, therefore biasing the models to predict a scenario of failure (positive I values).

Furthermore, if the critical loading conditions were to drive the material into a critical state, once the fatigue resistance limits are reduced, one could expect to see fatigue failures when carrying out the tests. This will either attest that the material is inadequate for the application and/or the design loads are too high for the given steel, or it will permit one to assess on the conservativeness of the involved criteria. Either way, the inspection of the critical loading conditions is expected to reveal interesting results.

2.4. Specimen geometry

The fatigue resistance limits were previously determined (Machado et al., 2020) with the geometry depicted in Fig. 6, where f_{-1}=357 MPa and t_{-1}=275 MPa correspond to the endurance limits under pure bending and pure torsion. In order to maintain consistency, the same geometry was chosen to the experiments within the present study.

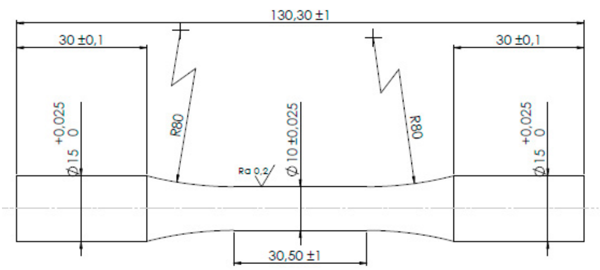

Fig. 6. Adopted specimen geometry

3. Results and discussion

The results relative to the FEM-extracted loading conditions are available in Table 6. As one can easily observe, all specimens regarding B06, B06', B03 and B03' managed to endure 10 million cycles without failure. This does not come across as a surprise, as the loading conditions were well within the elastic regime and well below the uniaxial fatigue resistance limits of the material.

Table 6. Experimental results for FEM-extracted loading conditions

DIN 42CrMo4							
Loading condition	σ_a [MPa]	σ_m [MPa]	τ_a [MPa]	τ_m [MPa]	β [°]	**Experiment 1 [cycles]**	**Experiment 2 [cycles]**
B03’	54.12	41.31	111.60	0	235	10 M	10 M
B06’	98.23	97.41	100.91	0	0	10 M	10 M
B03	95.43	0	111.60	0	235	10 M	10 M
B06	195.63	0	100.91	0	0	10 M	10 M

Given the fact that the other FEM-extracted loading conditions are less severe than the experimented ones, no further fatigue testing was required, as additional testing would only produce additional run-outs. Instead, the fatigue behaviour of the material can be securely assessed by discussing the error indices associated to each of the loading conditions.

Fig. 7 presents the yielded error indices for the respective loading conditions B03’, B05’, A06’, B06’, A07’ and B10’, i.e, FEM-extracted loading conditions considering a mean normal stress. Accordingly, Fig. 8 presents the yielded error indices for the fully reversed FEM-extracted loading conditions B03, B05, A06, B06, A07 and B10. The average of all error indices for each loading conditions are presented below each set of bar graphs.

As one would expect, all the loading conditions have yielded negative values of error indices, which is the condition where the fatigue resistance limits are greater than the driving forces to fatigue failure. Since the error indices are distant to nil, this indicates that the stresses to which the crankshaft was subjected in operation are adequate, not constituting a project design flaw.

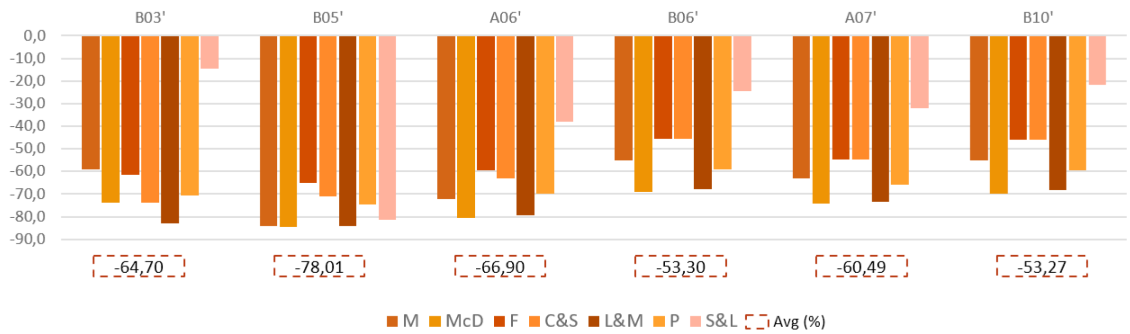

Fig. 7. Error indices for the FEM-extracted loading conditions including mean normal stress

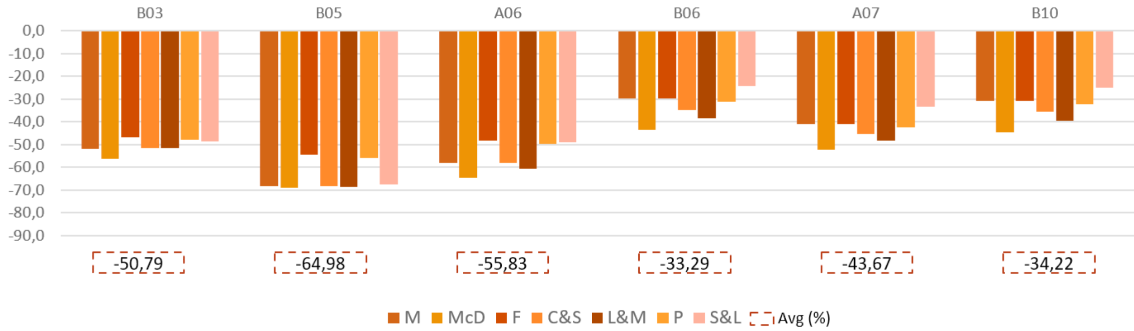

Fig. 8. Error indices for the fully reversed FEM-extracted loading conditions

The error indices relative to each loading condition provide the means to compare the prediction behaviour of the involved models. Regarding the loading conditions where normal mean stress is present (Fig. 7), the greatest *I* values correspond to approximately -45%. The only observed exception is that Susmel & Lazzarin's criterion yielded a significant number of error indices not so distant to zero. This can either indicate that the criterion is a lot more conservative in the presence of mean normal stress compared to the others, or that the presence of the mean normal stress exerts a negative influence on the output of this particular model.

Regarding the fully reversed FEM-extracted loading conditions (Fig. 8), clearly the error indices were slightly increased when compared to error indices yielded from the loading conditions that included mean normal stresses. This is a direct consequence of the fact that including a superimposed mean normal stress at the cost of reducing the applied normal stress amplitude should, in fact, be less severe in terms of fatigue failure to the component. As a matter of fact, in a uniaxial scenario, if one was to raise the mean normal stress to the yield stress and reduce the normal stress amplitude to zero, the component should be expected to present anything but fatigue failing. This behaviour was already expected, and this is the reason why fully reversed loading conditions were also considered in the first place.

Nevertheless, still the error indices are significantly low and far from a critical condition to failure. The highest values are relative to B06, being them around -30% for Matake and Findley, as well as -24% for Susmel & Lazzarin. The latter still presented *I* values that were more conservative compared to the predictions obtained from the other criteria, only this time the values are better aligned with the error indices obtained from the other models.

In terms of average values, all average values per loading conditions raised (became closer to zero) when the fully reversed loading conditions were considered. The most severe loading condition is B06, thus being the loading condition of most interest. The average shifted from -53% to -33%, which is still a safe condition to operate. Once again it is possible to conclude that the loads that the crankshaft experienced in its operation were adequate and the early observed failure is due to stress concentration possibly due to impurities within the material or to external localised damages that led to stress concentrations.

Relative to the critical loading conditions, due to experimental problems, 7 experiments were discarded because the fracture took place out of the reduced cross-section region. At the time of fracture, they all had experienced around 1.5M to 2M cycles, with one reaching up to 2.5 M cycles.

An updated geometry that required less pressure from the collet of the testing system has been proposed (still under evaluation), and the run-out limit was established at 5M cycles. The experimental results are summarised in Table 7. Columns "experiment 1" and "experiment 2" are relative to the old geometry, while "experiment 3" is relative to the new geometry, which is still under evaluation.

Table 7. Experimental results for critical loading conditions

DIN 42CrMo4								
Loading condition	σ_a [MPa]	σ_m [MPa]	τ_a [MPa]	τ_m [MPa]	β [°]	**Experiment 1 [cycles]**	**Experiment 2 [cycles]**	**Experiment 3 [cycles]**
A	328	0	157	0	0			5 M
B	286	0	137	0	90	140 k	10 M	
C	233	0	224	0	0	10 M	2.4 M	3 M (still running)
D	213	0	205	0	90	10 M		
H	280	280	134	0	0			1 M (still running)

Two failures (B1 and C2) were observed, while B2, C1 and D1 outlived 10M cycles. The new geometry indeed required less pressure from the collet, and A3 managed to outlive 5M cycles. Up to the present moment, C3 and H3 are still running. The discarded experiments were relative to A1, A2, D2, E1, E2, H1 and H2.

Since the fatigue experiments were limited to one order of magnitude above the expected fatigue-life for the critical conditions, run-outs were not to be expected. Furthermore, the error indices predicted a slight predominance of positive *I* values, as can be seen in Fig. 9, which suggests that fatigue failures should eventually take place within the 10M cycles.

Findley predicted significantly high (positive) *I* values for loading conditions H (52%) and I (46%), which are the ones considering a superimposed mean normal stress. Loading conditions E, F and G consider a superimposed mean shear stress, where Matake's prediction was as high as 39% for loading condition G.

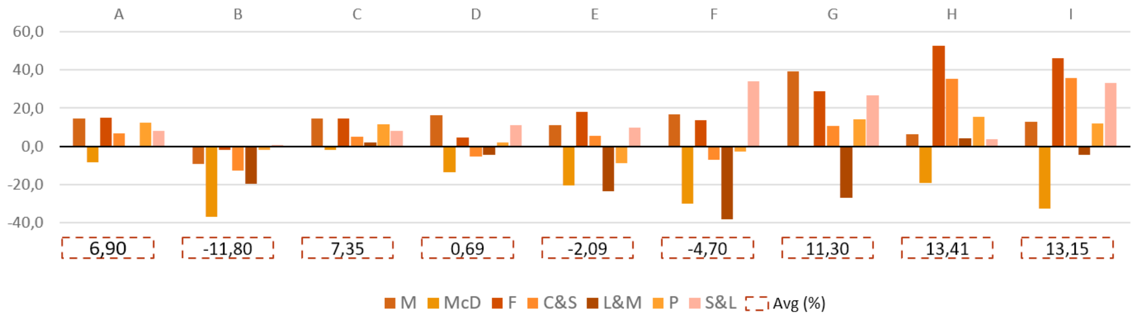

Fig. 9. Error indices relative to the critical loading conditions

On the other hand, significantly low predictions were delivered by Liu & Mahadevan (loading conditions F and G) and by McDiarmid (loading conditions B, F and I). This can indicate a non-conservative behaviour of the given models, once they might indicate that loads can be increased, what may lead the material into fatigue failure.

The behaviour of the predictions relative to each model was summarised in Fig. 10, where each criterion is represented by the average of its own error indices. Averages located within the ±10% range are considered to be ideal, and positive values may be desirable as it indicates a slight biasing of the given model towards a conservative prediction behaviour. It is also important to mention that the criteria which did not meet the targeted ±10% are not necessarily inadequate, as this is an assessment of the criteria's prediction behaviour within the context of this particular material including its own characteristics of metallurgy and mechanical properties.

With that being said, the present study has observed that Papadopoulos' criterion was the one to present the best overall performance, not only because its average is the closest to nil, but also because of its positive average which indicates a slight tendency towards conservativeness. In addition, the fact that it does not require critical plane determination is also an attractive characteristic, making its use a lot friendlier.

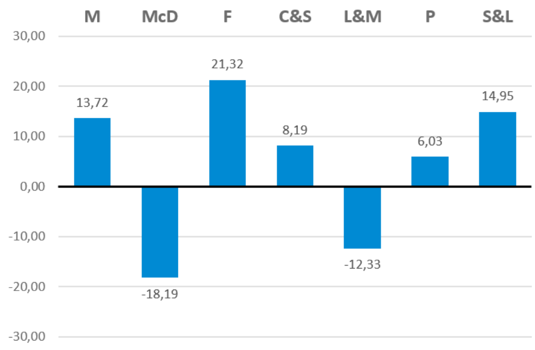

Fig. 10. Summary of the average of error indices relative to each individual criterion

4. Conclusions

Based on what is presented above, the following conclusions can be drawn:

- The present study established a procedure to translate non-trivial stress states into a set of combined bending and torsion loading conditions that can be experimented in laboratory.
- All FEM-extracted loading conditions yielded run-outs, indicating that the stresses observed in operation are adequate for the material in which the crankshaft is forged.
- The FEM-extracted loading conditions yielded very negative error indices, which is in good agreement with the experimental observations, endorsing the idea that the designed loads are adequate to this particular material and, by themselves, do not constitute a design flaw.
- Still relative to the FEM-extracted loading conditions, the error indices shifted to higher values (still negative) once the mean normal stress was disconsidered yielding a larger normal stress amplitude. In addition, the conservative behaviour of Susmel & Lazzarin was attenuated, revealing a better alignment with the other criteria's prediction.
- Despite experimental issues, critical loading conditions were considered, and run-out events were observed even though the run-out limit was set to one order of magnitude greater than the expected fatigue-life.
- Error indices relative to the critical loading conditions were determined considering experimentally measured fatigue resistance limits. The error indices were therefore biased to fatigue failure predicting, but still remained close to zero. Such tendency to failure was not verified in experimental observations, where run-out events were observed.
- Comparing the criteria's predicting capability, Papadopoulos' criterion yielded the least spread throughout the different loading conditions, presented the closest to nil average while still being adequately conservative. Its ease of use is also an interesting feature that endorses its use.

Acknowledgements

This research was developed within the scope of the research and Technological Development of the Brazilian Electric Energy Sector Program regulated by ANEEL, with the support of the Eneva Companies - Pecém II Energy Generation S.A., Itaqui Energy Generation S.A., Parnaíba Energy Generation and Commercialization S.A. and Parnaíba II Energy Generation S.A.

References

Carpinteri, A., & Spagnoli, A. (2001). Multiaxial high-cycle fatigue criterion for hard metals. *International Journal of Fatigue*, *23*(2), 135–145. https://doi.org/10.1016/S0142-1123(00)00075-X

Castro, T. L. (2019). *Previsão da Vida em Fadiga de Eixos Virabrequim e Componentes Mecânicos Estruturais sob Carregamento Multiaxial*. PUC-Rio.

Findley, W. N. (1959). A Theory for the Effect of Mean Stress on Fatigue of Metals Under Combined Torsion and Axial Load or Bending. *Journal of Engineering for Industry*, *81*(4), 301–305. https://doi.org/10.1115/1.4008327

Liu, Y., & Mahadevan, S. (2005). Multiaxial high-cycle fatigue criterion and life prediction for metals. *International Journal of Fatigue*, *27*(7), 790–800. https://doi.org/10.1016/j.ijfatigue.2005.01.003

Machado, P. V. S., Araújo, L. C., Soares, M. V., Reis, L., & Araújo, J. A. (2020). Multiaxial fatigue assessment of steels with non-metallic inclusions by means of adapted critical plane criteria. *Theoretical and Applied Fracture Mechanics*, *108*(March), 102585. https://doi.org/10.1016/j.tafmec.2020.102585

Marquis, G. B., & Socie, D. F. (2000). *Multiaxial Fatigue*. SAE International. https://doi.org/10.1016/B0-08-043749-4/04030-1

Matake, T. (1977). Explanation on Fatigue Limit Under Combined Stress. *Bull JSME*, *20*(141), 257–264. https://doi.org/10.1299/jsme1958.20.257

McDiarmid, D. L. (1987). Fatigue Under Out-of-Phase Bending and Torsion. *Fatigue & Fracture of Engineering Materials & Structures*, *9*(6), 457–475. https://doi.org/10.1111/j.1460-2695.1987.tb00471.x

Papadopoulos, I. V., Davoli, P., Gorla, C., Filippini, M., & Bernasconi, A. (1997). A comparative study of multiaxial high-cycle fatigue criteria for metals. *International Journal of Fatigue*, *19*(3), 219–235. https://doi.org/10.1016/S0142-1123(96)00064-3

Peixoto, T. A. (2018). *Interação entre Aspectos Microestruturais e Iniciação de Trincas de Fadiga em Aços Estruturais*. PUC-Rio.

Schijve, J. (2009). Fatigue of structures and materials. In *Fatigue of Structures and Materials*. https://doi.org/10.1007/978-1-4020-6808-9

Schwaben. (2015). *Finite element analysis for stress determination acting on crankshaft in Brazilian thermoelectric powerplant - Private report*.

Suresh, S. (1998). Fatigue of Materials. In *Fatigue of Materials*. https://doi.org/10.1017/cbo9780511806575

Susmel, L., & Lazzarin, P. (2002). A bi-parametric Wöhler curve for high cycle multiaxial fatigue assessment. *Fatigue and Fracture of Engineering Materials and Structures*, *25*(1), 63–78. https://doi.org/10.1046/j.1460-2695.2002.00462.x

Zenner, H., Heidenreich, R., & Richter, I. (1985). Dauerschwingfestigkeit bei nichtsynchroner mehrachsiger Beanspruchung. *Materialwissenschaft Und Werkstofftechnik*. https://doi.org/10.1002/mawe.19850160310